Wind Tunnel Wall Corrections Deduced by Iterating from Measured Wall Static Pressure

D.F. Moses*
San Diego State University, San Diego, California

An iterative method for calculating wall interference corrections to model lift and induced drag from simple flowfield measurements is presented. The method is applied to low-speed solid-wall wind tunnels, where the only measurements required are wall static pressures. The procedure for the iterations is described and the criterion for convergence to unconfined flow is given. The advantages of this method are that it easily handles cases having strong viscous effects, models with running propellers, etc. The viability of the procedure is demonstrated in a low-speed wind tunnel test of a wing model. A comparison shows that the standard method of images undercorrects, in this particular case, by about 20-30%.

Nomenclature

A_{ij} = transformation matrix between μ_j and ϕ_i
A'_{ij} = matrix analogous to A_{ij} for inner flow region
b = geometric span of the wing model
B_{ij} = transformation matrix between μ_j and v_i
B'_{ij} = matrix analogous to B_{ij} for inner flow region
$\bar{c}$ = chord of the wing model
c_ℓ = local lift coefficient of the finite-span wing model
C_L = lift coefficient of the finite-span wing model
D_{ind} = induced drag of the wing model
k = relaxation factor determining how much of the error signal is added to $v_i^{(n)}$ for the next iteration
N = number of points where $\hat{p}_i$ is measured
p_i = static pressure at the ith boundary value point in S
$\hat{p}_i$ = perturbation pressure at the ith boundary value point in S
p_∞ = static pressure of the undisturbed stream
S = imaginary, cylindrical surface surrounding the model in the near field
u_i = x component of perturbation velocity at the ith control point in the region 1 flow description
U_∞ = velocity of undisturbed stream
v_i = velocity component normal to S at the ith boundary value point in the outer flow
v'_i = velocity analogous to v_i for inner flow
v_{mi} = measured values of v'_i
w = z component of velocity (due to walls)
α = wing model angle of attack
Γ = strength of a vortex (segment)
ϵ = criterion for convergence of iterative flow computations, e.g., $\delta^{(n)} v_i \leq \epsilon$
μ_i = dipole strength of the ith element in the region 1 flow description
μ'_i = dipole strength of the ith element in the region 2 flow description
ρ = air mass density, assumed constant
ϕ_i = perturbation velocity potential at the ith control point in the outer flow (that which remains when the velocity potential of the undisturbed stream is subtracted from the total velocity potential)
ϕ'_i = velocity potential for the inner flow
ϕ_{mi} = values of ϕ_i obtained from the measured $\hat{p}_i$

Superscripts
(n) = iteration number
(N) = number of iterations to obtain $\delta^{(n)} v \leq \epsilon$

Subscripts
i,j = indices referring to the boundary value points distributed in S
m = measured values

Introduction

An accurate handling of wind tunnel wall corrections has received attention in recent times for at least two reasons. First, in a time of increased power costs, an accurate determination of the wall correction can allow the use of larger models which would otherwise require larger (more expensive to operate) tunnels. Second, demands for greater accuracy in aircraft performance predictions place corresponding demands on the accuracy of wind tunnel results. Until comparatively recently, wall interference was calculated using singularity methods,[1-3] e.g., "image" methods. These methods have well-known disadvantages, such as 1) that complicated models are not easily modeled in terms of simple singularities; 2) that the flow about large models may be affected by the wall boundary layers, which obviously are not accounted for in potential flow; and 3) that rotors, propellers, jets, and wakes are also difficult to simulate.

Wall corrections were made essentially in this way until the adaptive wall concept was introduced by Ferri and Baronti[4] and by Sears.[5]

As an alternative to the method of images, flow variables can be measured in the surface of an imaginary cylinder containing the model. These measurements can then be used to define the total flowfield (the sum of all perturbation fields plus the onset flow, since the problem is linear), which, by a process of iteration, can be transformed into the flow about the model in unconfined flow. The advantages of this method are that model complexity offers no problem, it accounts for boundary layers, wakes, running propellers, etc., with little difficulty. It is the purpose of this work to demonstrate this alternate method by applying it to a wind tunnel test of a wing model having a span-to-tunnel-width ratio of 0.75.

The present method may be thought of as a simulation of the "adaptive-wall" scheme. In that scheme, the mismatch between the flow in the tunnel and a computed, outer flow is used to modify the tunnel's walls to produce the unique

Received Aug. 10, 1982; revision received March 25, 1983.

*Associate Professor of Aerospace Engineering. Member AIAA.

flowfield that satisfies all the boundary conditions. In the present application, however, the tunnel's walls are not adjustable; the iterative procedure leading to unconfined conditions is therefore only a numerical simulation. The flow perturbations needed at the wall to produce unconfined flow are determined, and the resulting perturbations within the tunnel form the basis of the corrections applied to measured model data.

It is important to notice that the exterior flowfield is calculated from measured data at the interface—in this case, at the tunnel's walls. The field of extraneous velocities (the wall effect) determined by the method can be described in as much detail as desired, so that the corrections to be applied to model data can be calculated as simply or as elaborately as is appropriate.

The method presented has great generality; it is valid for any model and tunnel configuration within the approximation of linearity. For the special case of a solid-wall tunnel, as demonstrated here, it requires only the measurement of wall static pressures. For ventilated tunnels, it would require measurement of two flow variable distributions, but otherwise would be carried out exactly as presented here.

Thus the present paper is presented with two aims: first, to show how wall corrections can be made, within the linear regime, using data measured away from the model and thus providing improved accuracy for complex, viscous, powered configurations; and second, as a detailed practical proposal for use of operators of low-speed solid-wall tunnels.

Analysis

As in the adaptive wall case (as formulated by Sears[5]), the present method (for solid-wall tunnels) acts to establish, in the surface of a cylinder surrounding the model (the interface), values of flow variables that the model would produce in unconfined flow. Let the surface of this cylinder be called S, and, for convenience, let S take the location of the inside surface of the tunnel test section. S is an interface that divides the entire flowfield into inner and outer regions. The inner region is the region within the wind tunnel, including the model; its flow is the existing flow of the experiment carried out, but subject to correction for boundary interference. The outer flow exists only in numerical simulation, and always satisfies the correct boundary conditions in the far field, etc. Each region will be treated separately, but, clearly, when unconfined flow is reached, they must be compatible at S. The flow variables to be measured are chosen, in this treatment, to be perturbation pressure, $\hat{p}_i = p_\infty - p_i$, and the normal component of perturbation velocity, v_{mi}. Initially, the $\hat{p}_i$ serve as boundary conditions for the mathematical description of the flow in the outer region. The other condition is that the perturbation pressures vanish at large distances. Specifying the scalars $\hat{p}_i$ completely defines the outer flow, so that one can compute the corresponding v_i. Initially $v_i \neq v_{mi}$ in general. The discrepancy $v_i - v_{mi}$ is a measure of departure from unconfined flow. It, or a function of it, can now be used to modify the outer boundary conditions of the inner region, and thus to obtain a mathematical description of an improved flow in this region. The inner boundary conditions of this region are those imposed by the model and its wake. Specifying these boundary conditions defines the improved inner flow, from which the corresponding $\hat{p}_i$ can now be calculated. Using these new values as boundary conditions for the next approximation to the outer flow, another set of v_i are obtained, and so the iteration goes. We say that the iteration process has converged to unconfined flow when this error has diminished to a suitably small value. At convergence, the wall effect can be determined anywhere in the test section; it is the total flow perturbation there due to incremental changes of the inner-flow boundary values at all points of S.

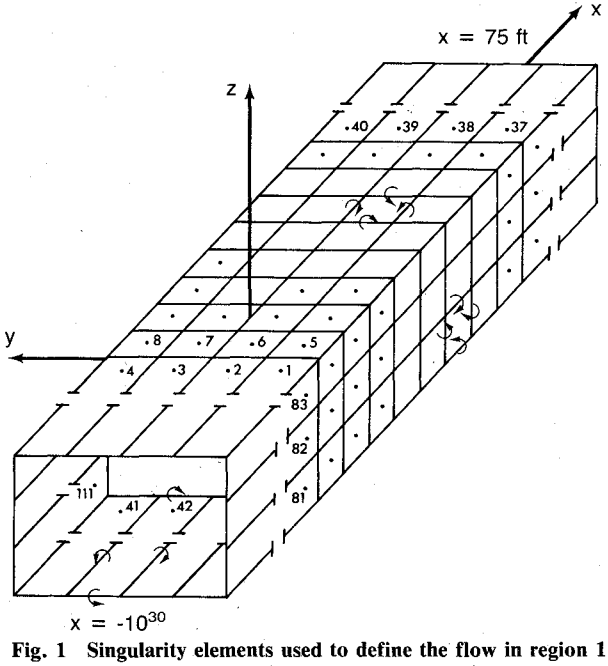

Fig. 1 Singularity elements used to define the flow in region 1 and their control points, numbering scheme, and coordinate system.

Far-Field Flow Region

The wind tunnel is assumed to operate at low speed, so that Laplace's equation applies outside of viscous regions. The flow in the far field, referred to as region 1, or the "outer region," will therefore be modeled by singularity distributions on S. In view of linearity, the analysis is most conveniently carried out using perturbation quantities.

The wind tunnel test section is replaced (in this problem) by 140 rectangular elements lying in the surface S, the inside surface of the test section, and each element is assumed to have an area distribution of constant (an exception to this will be mentioned shortly) but unknown dipole strength (see Fig. 1). In order to eliminate the possibility of a situation where a homogeneous solution of the flow equations is just a toroidal motion about S, the upstream-most elements are elongated to $-\infty$. The downstream-most elements are also elongated to $+\infty$ [actually to $x = 22.86$ m (75 ft) for computational purposes] in order to account for the flow induced by the trailing vortices of the wing model. Each element contains a point, located at its center (except for leading and trailing elements), referred to as the *boundary-value point,* or *control point,* where the boundary conditions are satisfied.

The exception to the constant-strength distribution is the upstream-most set of elements. The u distribution of, say, a wing model can be approximated by the u distribution of a line dipole at large distances.[6]

For these elements we then get

$$\mu_i(x) = \mu_i(x_C)\, m(x)$$

where x_C is the x coordinate of the ith control point, and $m(x)$ is the shape function, $1/x^2$. $\mu_i(x_C)$ therefore acts like a generalized coordinate.

In terms of its perturbation potential, we can express the flowfield in the outer region as

$$\phi_i = A(x,y,z)_{ij}\mu_j \tag{1}$$

where $A(x,y,z)$ is a matrix determined from geometric quantities according to the algorithm associated with the particular type of singularity,[7] and the summation convention is implied by the repeated subscript. For a dipole distribution we have

$$\phi_i = -\frac{1}{4\pi}\iint_S \frac{\mu(x,y,z)\cos\theta}{r_i^2}\,dS$$

where r is the distance from the elemental dS to the ith control point, and θ is the angle between r and the assumed dipole direction. Solving the linear system (1) need only be done once for a given wind tunnel. Knowing the μ_j's one can calculate any flow quantity of interest, in particular v_i, the perturbation velocity component normal to the surface S. We obtain

$$v_i = B(x,y,z)_{ij}\mu_j$$

In this equation, it is convenient to consider the rectangular singularity elements no longer as area-dipole distributions but to recognize them as vortex rings made up of four rectilinear vortex segments which form the element sides. The parameter μ_i is therefore recognized as the constant but unknown circulation of each of the element's vortex segments.

Near-Field Flow Region

The flowfield within S, referred to as region 2, is computed in a way similar to that of the outer region. For this treatment it is assumed that a wing is present and that it will be represented by four additional plane, horizontal dipole elements, which are elongated to $x=22.86$ m (75 ft) to represent the trailing vortices. Weissinger[8] showed that for best representation of a wing, the bound vortex of the element should be located at the quarter-chord point, and the control point at the three-quarter-chord point. Accordingly, the leading edges of the wing dipole elements are at $x=0$ m and the control points are at $x=0.076$ m (0.25 ft).

We denote inner-flow quantities by primes so that the velocity potential and normal component of velocity are given respectively by

$$\phi_i' = A_{ij}'\mu_j' \tag{2}$$

$$v_i' = B_{ij}'\mu_j' \tag{3}$$

The boundary condition at the wing is that the pressure distribution on the wing is held constant as the walls are removed; thus the wall effect manifests itself as a change in the model geometry (angle of attack, twist, camber, etc.). That is, as we iterate to unconfined flow, the angle of attack and/or the wing geometry are adjusted so as to keep the pressure distribution fixed. The wing boundary condition for this case, then states that $\delta\Gamma$, and therefore $\delta\mu$, for all wing elements is equal to zero at each iteration. (The reason for these incremental $\delta\mu$'s being used will become clear shortly.)

There is actually an alternative boundary condition; namely, one might require that the model geometry be fixed as we iterate to unconfined flow; then the wall correction appears as a change in the pressure distribution and velocity field of the wing. This is, to be sure, a better simulation of how an adaptive-wall tunnel works.

These two different wing boundary conditions yield different, but compatible results. The former is analogous to the way the classical image method is always carried out.[3] Moreover, it is clearly more accurate in modeling, by inviscid methods, flows with significant viscous effects. Since the wing boundary layer and wake are almost entirely dependent upon the pressure distribution, rather than the wing geometry per se, and since these viscous effects are not altered in the iteration to unconfined flow, it makes more sense to fix the pressure distribution. In this paper, therefore, we use only the first alternative. (Both alternatives are used and their results combined in Ref. 7.)

Having established the boundary conditions at the wing location, the remainder of the boundary conditions for the inner flow are specified at the 140 control points of the wall-singularity elements. These wall boundary conditions are the $v'^{(n+1)}$ determined from the outer flow in a manner to be specified below (n in this context refers to the iteration number).

It will be recalled that ϕ_{mi} is used to fix the outer-flow description from which the corresponding v is computed. If square brackets are used to denote the functional relationship in region 1, we can write this computed outer-flow normal velocity as $v[\phi_m]$. In general, the symbol $v[\phi'^{(n)}]$ will be used to denote the outer-flow normal-velocity component calculated from the values of the velocity potential $\phi'^{(n)}$ at the surface S in the nth iteration.

If we let $v'^{(1)} \equiv v_m'$, the measured velocity component perpendicular to S, we can write the discrepancy in v between inner- and outer-flow descriptions, in the first iteration, as

$$\delta^{(1)}v \equiv v[\phi_m] - v'^{(1)} \tag{4}$$

It is clear, at this point, that both measured functions, ϕ_m and v_m are needed, to proceed with this method, i.e., two functions must be measured at S, in general. For the special case of the solid-wall tunnel, neglecting boundary-layer growth, v_m is known because the wall slope is known (usually zero). The symbol $v'^{(1)}$ is therefore carried in Eq. (4) but is put equal to zero in the calculations carried out below, for the tests conducted at the University of Arizona. For the nth iteration we have the analogous definition

$$\delta^{(n)}v \equiv v[\phi'^{(n)}] - v'^{(n)} \tag{5}$$

where $v'^{(n)}$ is the (inner) normal velocity at S, and $v[\phi'^{(n)}]$ is the normal velocity calculated for region 1 using the potential $\phi'^{(n)}$. Equation (5) is referred to as the error signal at the nth iteration.

The boundary conditions at the wall-element control points at the beginning of the $(n+1)$th iteration are obtained by relaxing those existing at the beginning of the nth iteration; that is,

$$v'^{(n+1)} = v'^{(n)} + k\delta^{(n)}v \tag{6}$$

The relaxation factor k applied to the discrepancy signal, defined above, is here assumed, for simplicity, to be a constant for all elements and all iterations.

Since v_m is not measured at the wing, it is not known there, so that $v'^{(n+1)}$ will be unknown at this location for all n. However, since the governing equations are linear, we can do the iterative computations using only the increments. It then becomes unnecessary to know the values of the v_m at the wing control points. To be specific, we shall compute the *increments* of normal velocity $[\delta^{(n)}v' = k\delta^{(n)}v]$ and of velocity potential $[\delta^{(n)}\phi']$ in the successive iterations. This method renders the boundary-value problems for both regions 1 and 2 determinate. That this is true for region 2 follows from the definition of the wing boundary conditions given above: The increment $\delta^{(n)}\phi'$ cannot have any discontinuity at the wing location. This implies that we can simply ignore the wing elements for the inner flow computation.

Just as we have used square brackets to denote the functional relationship of the outer flow, let us now introduce braces to denote the functional relationship of the inner flow:

$$\phi'^{(n)} \equiv \phi\{v'^{(n)}\}$$

This notation means that the velocity potential ϕ' in the nth iteration is calculated from the boundary values v' imposed at the walls, together with the appropriate condition, as discussed above, at the wing location.

The linearity of our problem ensures that the same functional relationship exists between the increments:

$$\delta^{(n)}\phi' = \phi\{\delta^{(n)}v'\}$$

where

$$\phi'^{(n+1)} = \phi'^{(n)} + \delta^{(n)}\phi' \tag{7}$$

and

$$v'^{(n+1)} = v'^{(n)} + \delta_i^{(n)}v'$$

$$= v'^{(n)} + k\delta^{(n)}v \tag{8}$$

Clearly,

$$\delta^{(n)}\phi' = \phi\{k\delta^{(n)}v\} = k\phi\{\delta^{(n)}v\}$$

This result is obtained by solving the linear system [Eq. (3)]

$$B'_{ij}\delta^{(I)}\mu'_j = k\delta^{(I)}v_i$$

for $\delta^{(I)}\mu'_j$ and then computing $\delta^{(I)}\phi'_i$ from [Eq. (2)]

$$\delta^{(I)}\phi'_i = A'_{ij}\delta^{(I)}\mu'_j$$

The above $\delta^{(I)}\phi'_i$ values are now used as updated boundary conditions for the outer-flow description, replacing ϕ_m.

Iteration to Unconfined Flow

The preceding two sections have essentially dealt with one typical iteration in the process leading to unconfined flow conditions for a model and its support system. We will now consider the convergence of this process.

Equation (5) gives the general definition of the error signal, which takes the form of Eq. (4) for the first iteration. We require, however, a recurrence relation between successive δv's. Professor Sears has provided this; it is derived as follows, using the notation introduced above and invoking linearity of the operation denoted by [ ]:

$$\begin{aligned}\delta^{(n)}v &= v[\phi^{(n)}] - v^{(n)}\\ &= v[\phi^{(n-1)} + \delta^{(n-1)}\phi] - v^{(n-1)} - k\delta^{(n-1)}v\\ &= v[\delta^{(n-1)}\phi] + v[\phi^{(n-1)}] - v^{(n-1)} - k\delta^{(n-1)}v\\ &= v[\delta^{(n-1)}\phi] + (1-k)\delta^{(n-1)}v\end{aligned}$$

where, it will be recalled, $\delta^{(n-1)}\phi$ is just $k\phi\{\delta^{(n-1)}v\}$. Sears' recurrence formula therefore states that $\delta^{(n)}v$ is obtained from $\delta^{(n-1)}v$ by application of the linear operator

$$1-k+v[k\phi\{\ \ \}]$$

It will be understood that an iteration ends and the next one begins at the point where the computation moves from region 1 to region 2.

The iteration of the flow computation between the two regions continues until $\delta^{(n)}v$ becomes sufficiently small, i.e., $\delta^{(n)}v < \epsilon$. For the present case we choose $\epsilon = 0.015$ m/s (0.05 ft/s). At this point we say that we have reached unconfined-flow conditions, since, from Eq. (5),

$$0 \doteq v[\phi'^{(n)}] - v'^{(n)}$$

therefore

$$v[\phi'^{(n)}] = v'^{(n)}$$

We see that the velocity component normal to S (as well as the velocity potential) is the same for outer and inner flows at all points on S. This situation means that we have converged to unconfined flow.

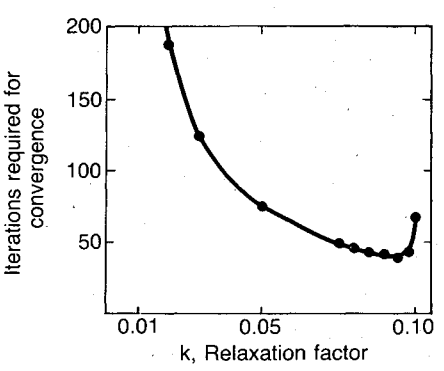

Fig. 2 Effect of the value of k on the rate of convergence (using measured values of $\hat{p}_i$).

Equation (8) may be written as

$$v'^{(n)} = v'^{(n-1)} + \delta^{(n-1)}v'$$

Repeated substitution for the first term on the right-hand side of the equation gives

$$v_i'^{(N)} = v_i^{(I)} + \sum_{n=1}^{N-1}\delta^{(n)}v_i'$$

$$v_i^{(N)} = v_{mi} + \sum_{n=1}^{N-1}k\delta^{(n)}v_i \qquad (9)$$

where $v_i^{(N)}$ is the value of the total normal perturbation velocity at control points i for unconfined flow. Likewise, we can write Eq. (7) as

$$\phi'^{(N)} = \phi'^{(N-1)} + \delta^{(N-1)}\phi'$$

Again, after repeated substitution for the first term on the right, we obtain the total perturbation velocity potential for unconfined flow:

$$\phi_i^{(N)} = \phi_{mi} + \sum_{n=1}^{N-1}\delta^{(n)}\phi_i \qquad (10)$$

The wall effect is that which is added to the initial values of the flow parameters (measured or deduced from measured values) to get unconfined flow. In Eq. (9), the term

$$\sum_{n=1}^{N-1}k\delta^{(n)}v_i$$

is therefore the wall correction to the normal perturbation velocity at points i, and the term

$$\sum_{n=1}^{N-1}\delta^{(n)}\phi_i$$

is the wall effect on the perturbation velocity potential at points i.

In the above discussion, k was assumed to be constant. For iterative wall-correction procedures applied to two-dimensional flow, it has been shown that the optimum (requiring fewest iterations to convergence) value of k is approximately ½. However, in our three-dimensional case, it was found that the process diverged for any $k \geq 0.10$. Figure 2 shows the number of iterations required for convergence as a function of the value of k. Clearly, the optimum for our case is somewhere in the range $0.09 \leq k \leq 0.0975$. It was also found that the error signal oscillated in the converging process for any $k > 0.02$. Figure 3a shows how these oscillations grow with increasing k until they become unstable and the process diverges. It can also be seen that the oscillations dampen out earlier for smaller values of k. In Fig. 3b, the "mean value" of $\delta^{(n)}v$ is converging faster for $k = 0.10$ than for either $k = 0.05$ or 0.08. It can also be seen that $k = 0.08$ is converging faster than $k = 0.05$ and, in fact, reaches zero after fewer iterations. (Figures 2 and 3 were obtained using measured $\hat{p}_i$.) It is known that the maximum value of $|\delta^{(n)}v_i|$ does not occur at the same value of i in each successive iteration. It is therefore apparent that the *distribution* of v_i changes from iteration to iteration. This change in distribution may be the reason why a small k and many iterations are required for convergence. The next best thing to a k function that could account for distribution may be some schedule for k that selects larger values for early iterations to accelerate the convergence and then smaller values later on. Such a schedule has not yet been determined.†

†Since this work was carried out, Dowell[9] has presented a method for determining the wall correction in one step, without the need for iterating. Dowell's observation is useful but not necessary in this wall-correction method. The iterative procedure is sufficient to prove out the method reported in this paper.

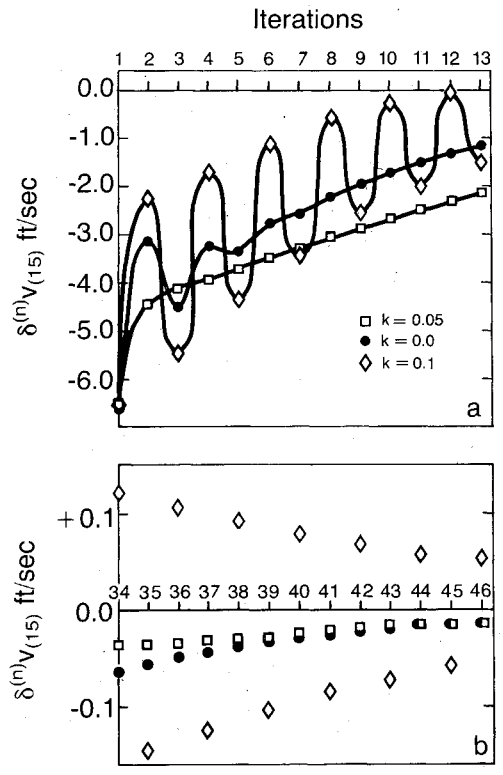

Fig. 3 Effect of the value of k on the error signal at $i=15$ over 46 iterations. a) Error signal for iterations 1-13. b) Error signal for iterations 34-46. Curves are drawn in for clarity. $U_\infty = 33.89$ m/s (111.19 ft/s).

Our wing boundary conditions assumed that the pressure distribution on the wing is unchanged and the wall correction is interpreted as a change of angle of attack, $\Delta\alpha$. From Eq. (9), the wall effect on the normal velocity component at the wing location is

$$\sum_{n=1}^{N-1} k\delta^{(n)} v_i, \qquad i=141,\ldots,144$$

The wall correction to the angle of attack is therefore

$$\Delta\alpha = \frac{1}{4} \sum_{i=141}^{144} \sum_{n=1}^{N-1} k\delta^{(n)} v_i / U_\infty \tag{11}$$

Before actually applying the method to a wind tunnel test, the FORTRAN program which was written to compute the wall corrections from the $\hat{p}_i$ values was used on a numerical test case. This test gave satisfactory results. Another test case included a distribution of small but nonzero values for v_m, and it was seen that this small deviation from $v_m = 0$, representing, perhaps, boundary-layer growth, had a negligible effect.

The Experiment

A wing model of aspect ratio 6, NACA 4418 section, was tested in the University of Arizona low-speed wind tunnel. (The tunnel has parallel, solid walls.) The span-to-width ratio was 0.75, and the wing was at the center position of the $1.21 \times 0.86 \times 3.05$ m ($48 \times 34 \times 120$ in.) rectangular test section. Forty-two static-pressure taps were distributed in the test section floor and ceiling, and four were located in the two sides. $\hat{p}_I$ was measured for $i = 1$-46 directly with a Baratron capacitance-type differential transducer by connecting one port to p_∞ far upstream and the other to a manifold. The 46 wall static pressures were connected to this manifold, each with a normally closed, tight-fitting tubing clamp. The $\hat{p}_i$ values were therefore measured by successively opening each clamp in turn and recording the transducer output on a strip chart. This method of measurement proved to be very accurate and repeatable. Runs were made with $U_\infty = 33.89$ m/s (111.19 ft/s) (Reynolds number = 300,000) at two angles of attack, 2 deg (run I) and 10 deg (runs G and H). Runs G and H were made on different days at the same conditions and were used to check repeatability. The lift was measured in each case by means of a Kasari strain-gage balance.

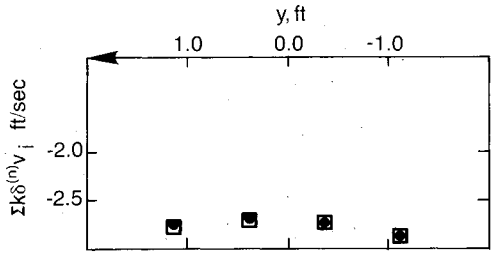

Fig. 4 Wall correction to v_i, $\sum_{n=1}^{N-1} k\delta^{(n)} v_i$ ($\alpha = 10$ deg), at the four wing-element control points for runs G (●) and H (□).

Table 1 Wall correction at a typical tail position

Wing C_L	Tail $\Delta\alpha$, deg	Wing α, deg	Silverstein and White[3] tail $\Delta\alpha$, deg
1.19	2.036	10	1.855
1.24	2.040	10	1.933
0.557	0.983	2	0.872

Table 2 Wall effect on the model induced drag

Wing α, deg	10	10	2
$\Delta C_{D_{\text{ind}}}$	0.0311	0.0312	0.0070

Wall Correction to the Model Measurements

The perturbation pressures, $\hat{p}_i$, measured during runs G, H, and I were input to the wall correction program. Figure 4 shows the wall correction at the locations of the four wing-element control points for runs G and H. It can be seen that the small differences in the data measured at the same conditions on different days have negligible effect on the final answer. Figure 5 contains the wall corrections for run I.

The wall corrections to the measured lift at the wing center can be calculated using Eq. (11). The results are plotted in Fig. 6.

Figure 6 also contains the wall corrections for this wing test computed by the conventional method of images as described by Silverstein and White.[3] It is seen that the method of images results in a correction about 20 or 30% smaller than the present technique.

It is not possible to compare these results with exact, "correct" values, which would have to be obtained from tests of the same wing at the same Reynolds number in a very large wind tunnel (or an adaptable tunnel). Such data do not exist. What can be claimed for the present technique is that its results are obtained from actually satisfying the boundary conditions, both at the wing and at the tunnel walls, albeit in the inviscid small-perturbation sense, in the presence of the existing viscous effects. Since the wall corrections are relatively small, we believe that this approximation is well justified and provides corrected experimental results of high accuracy. It is therefore reasonable to interpret Fig. 6 as evidence that the classical image technique underestimates the α correction, probably by 20 to 30%.

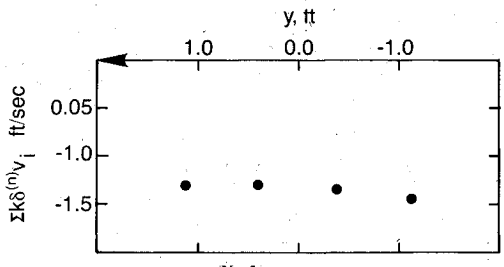

Fig. 5 Wall correction to v_i, $\sum_{n=1}^{N-1} k\delta^{(n)} v_i(\alpha=2$ deg), at the four wing-element control points for run I.

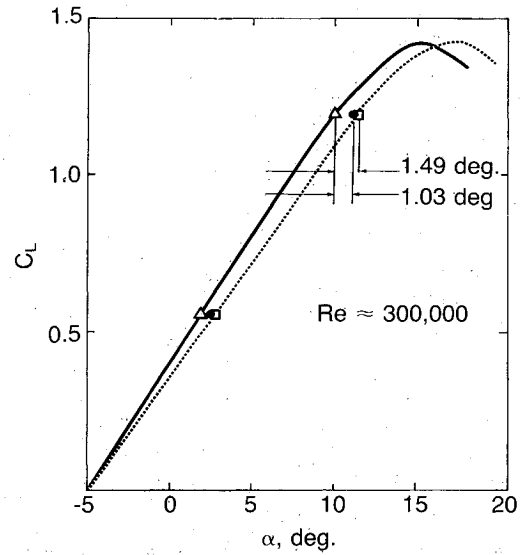

Fig. 6 Wall correcton to the measured lift curve of the wind tunnel model: △ measured on an NACA 4418, aspect ratio = 6 wing; □ wall correction from present method; • correction calculated from Silverstein and White.

Since there was no model tail surface and hence no singularity elements representing a tail surface, the only correction that was computed was that to the angle of attack at a typical tail position. The wall-correction program was used to calculated $\Delta\alpha$ at a point on the x axis one-half the geometric span downstream of the origin from the equation.

$$\Delta\alpha = \frac{1}{U_\infty} \sum_{n=1}^{N-1} k\delta^{(n)} v_{145}$$

in which v_{145} denotes the vertical velocity component at this typical tail position. The results of these calculations are contained in Table 1 along with the wall correction estimated from Silverstein and White.[3]

It may be observed that the $\Delta\alpha$'s from Fig. 4 and Table 1 can be used to determine a wall correction to the measured pitching moment of a model with tail. As the tail position approaches the wing quarter-chord, the pitching moment correction, of course, goes to zero.

Extraneous velocities are removed as we iterate to unconfined flow; therefore, a correction to the induced drag must be made. In general, for a lifting-line configuration, we have

$$\Delta D_{\text{ind}} = \rho \int_{-b/2}^{b/2} \Delta(-\Gamma w)\,dy$$

where w is the z component of velocity at the model quarter-chord. The negative sign is necessary because downwash is in the negative z direction. Substituting for Γ and dividing through by $\frac{1}{2}\rho U_\infty^2 \bar{c} b$, we get

$$\Delta C_{D_{\text{ind}}} = \frac{1}{b} \int_{-b/2}^{b/2} \Delta\left[-c_\ell \frac{w}{U_\infty}\right] dy$$

in which c_ℓ is the local lift coefficient of the model.

During the iteration, the model C_L is held constant so that the wall effect manifests itself in a change of downwash at the wing. The above expression then becomes

$$\Delta C_{D_{\text{ind}}} = \frac{1}{b} \int_{-b/2}^{b/2} -c_\ell \Delta\left[\frac{w}{U_\infty}\right] dy$$

$$= -\frac{1}{b} \int_{-b/2}^{b/2} c_\ell \Delta\alpha\, dy$$

where

$$\Delta\alpha = -\frac{\Delta w}{U_\infty} = -\frac{1}{U_\infty} \sum_{n=1}^{N-1} k\delta^{(n)} v$$

(It will be recalled that

$$\Delta w = \sum k\delta^{(n)} v$$

is the increment of upwash at the wing due to the singularity distribution, i.e., due to the wall removal, typically negative—while $\Delta\alpha$ is the corresponding change in α required to maintain constant lift.)

Here we might simply take c_ℓ and w/U_∞ to be average values and calculate $\Delta C_{D_{\text{ind}}}$ as C_L times the α correction obtained above. However, the calculation affords an opportunity to demonstrate how the detailed flowfield increments provided by this present method can be used more precisely. We can approximate the above integral as a sum evaluated at the four wing-element control points and obtain

$$\Delta C_{D_{\text{ind}}} = \frac{1}{b} \sum_{i=141}^{144} c_{\ell i} \Delta\alpha_i \frac{b}{4}$$

$c_{\ell i}$ is obtained from the theoretical lift distribution (Glauert[10]), for a wing of this planform. Table 2 contains the wall effect on induced drag. As the reader can verify, these values are virtually the same as those obtained by multiplying C_L by the $\Delta\alpha$ obtained previously.

Again it is impossible to compare these results with exact, "correct" results for this wing at the Reynolds number used. Our results are, of course, larger than would be predicted by classical image methods, which give $\Delta C_{D_{\text{ind}}}$ as simply the product of C_L times the (underestimated) $\Delta\alpha$ discussed above in connection with Fig. 6.

Conclusions

As stated in the Introduction, the purpose of this work was to demonstrate the feasibility of a more accurate method of making wall interference corrections for tests in solid-wall wind tunnels. To this end, a procedure was developed to calculate corrections based on measured flowfield quantities, such as static pressures measured at tunnel walls. This iterative process is seen to converge, for a suitably chosen relaxation factor k, in typically 45 iterations requiring approximately 30 s on a CYBER 175. For the model tested, being oversized and having a separated wake at high angles of attack, this method predicts, for example, a 20-30% greater correction of angle of attack than that given by the standard method of images.

It was found that for this three-dimensional situation the relaxation factor k needed to be much smaller for convergence ($k<0.11$) than would be inferred from two-dimensional results. The reason is probably that, since the error signal

$\delta^{(n)} v_i$ is distributed rather than being a constant, if a constant k is used then it is required to underrelax at each iteration in order to converge.

It should also be pointed out that it is not necessary to have a CYBER 175 or equivalent computer in order to use this method, since software techniques exist which will allow the computations to be accomplished on a minicomputer with external storage.

Acknowledgments

The work reported here was performed under supervision of Prof. W.R. Sears, who suggested the problem, while the author was a graduate student at the University of Arizona. Computer facilities and technician time were provided by the Aerospace and Mechanical Engineering Department of the University of Arizona.

References

[1] Theordorsen, T., "The Theory of Wind Wall Interference," NACA Rept. 410, 1931.

[2] Rosenhead, L., "Interference Due to Walls of a Wind Tunnel," *Proceedings of the Royal Society, Series A,* Vol. 142, 1933, pp. 308-321.

[3] Silverstein, A. and White, J.A., "Wind-Tunnel Interference with Particular Reference to Off-Center Positions of the Wing and to the Downwash at the Tail," NACA Rept. 547, 1935, pp. 135-147.

[4] Ferri, A. and Baronti, P., "A Method for Transonic Wind Tunnel Corrections," *AIAA Journal,* Vol. 11, Jan. 1973, pp. 63-66.

[5] Sears, W.R., "Self Correcting Wind Tunnels," *Aeronautical Quarterly,* Feb./March 1974, pp. 80-89.

[6] Prandtl, L. and Tietjens, O.G., *Applied Hydro- and Aero-Mechanics,* Dover Publications, New York, 1934, Chap. 6.

[7] Moses, D.F., "An Improved Method for Wind-Tunnel Wall Corrections Deduced by Iterating from Measured Wall Static-Pressure," Ph.D. Thesis, University of Arizona, Tucson, Ariz., 1980.

[8] Weissinger, J., "The Lift Distribution of Swept-Back Wings," NACA TM 1120, March 1947.

[9] Dowell, E.H., "Control Laws for Adaptive Wind Tunnels," *AIAA Journal,* Vol. 19, Nov. 1981, pp. 1486-1488.

[10] Glauert, H., *The Elements of Airfoil and Airscrew Theory,* Cambridge University Press, New York, 1923.